minerals

MDPI

Article

Cld-St-And-Bearing Assemblages in the Central Southalpine Basement: Markers of an Evolving Thermal Regime during Variscan Convergence

Marco Filippi [1,2,*], Maria Iole Spalla [1], Nicola Pigazzini [1], Valeria Diella [3], Jean-Marc Lardeaux [2,4] and Davide Zanoni [1]

1 Dipartimento di Scienze della Terra "A. Desio", Università degli Studi di Milano, 20133 Milano, Italy; iole.spalla@unimi.it (M.I.S.); n.pigazzini@arpalombardia.it (N.P.); Davide.Zanoni@unimi.it (D.Z.)
2 UMR Géoazur, Observatoire de la Côte d'Azur, CNRS, IRD, Université Côte d'Azur, 06560 Valbonne, France; lardeaux@unice.fr
3 Instituto di Geologia Ambientale e Geoingegneria (IGAG), Sezione di Milano, Consiglio Nazionale delle Ricerche, 20133 Milano, Italy; valeria.diella@cnr.it
4 Centre for Lithospheric Research, Czech Geological Survey, 118 21 Prague, Czech Republic
* Correspondence: marco.filippi@unmi.it

Abstract: Multiscale structural analysis was carried out to explore the sequence of superposed pre-Alpine chloritoid–staurolite–andalusite metamorphic assemblages in the polydeformed Variscan basement of the upper Val Camonica, in the central Southalpine domain. The dominant fabric in the upper Val Camonica basement is the late-Variscan S2 foliation, marked by greenschist facies minerals and truncated by the base of Permian siliciclastic sequences. The intersection with the sedimentary strata defines a Permianage limit on the pre-Alpine tectonometamorphic evolution and exhumation of the Variscan basement. The detailed structural survey revealed that the older S1 foliation was locally preserved in low-strained domains. S1 is a composite fabric resulting from combining S1a and S1b: in the metapelites, S1a was supported by chloritoid, garnet, and biotite and developed before S1b, which was marked by staurolite, garnet, and biotite. S1a and S1b developed at intermediate pressure amphibolite facies conditions during the Variscan convergence, S1a at T = 520–550 °C and P ≃ 0.8 GPa, S1b at T = 550–650 °C and P = 0.4–0.7 GPa. The special feature of the upper Val Camonica metapelites is andalusite, which formed between the late D1b and early D2 tectonic events. Andalusite developed at T = 520–580 °C and P = 0.2–0.4 GPa in pre-Permian times, after the peak of the Variscan collision and before the exhumation of the Variscan basement and the subsequent deposition of the Permian covers. It follows that the upper Val Camonica andalusite has a different age and tectonic significance as compared to that of other pre-Alpine andalusite occurrences in the Alps, where andalusite mostly developed during exhumation of high-temperature basement rocks in Permian–Triassic times.

Keywords: Variscan subduction/collision; pre-Alpine andalusite; chloritoid–staurolite metapelites

Citation: Filippi, M.; Spalla, M.I.; Pigazzini, N.; Diella, V.; Lardeaux, J.-M.; Zanoni, D. Cld-St-And-Bearing Assemblages in the Central Southalpine Basement: Markers of an Evolving Thermal Regime during Variscan Convergence. *Minerals* **2021**, *11*, 1124. https://doi.org/10.3390/min11101124

Academic Editor: José Francisco Molina

Received: 24 August 2021
Accepted: 7 October 2021
Published: 13 October 2021

1. Introduction

Andalusite is an indicator of high thermal regimes, such as those characterizing contact metamorphism or regional Buchan/Abukuma-type metamorphism in the metapelites of the continental crust [1,2]. High T/P ratios accountable for andalusite development are envisaged in various convergent and divergent settings, including late-orogenic thinning and lithospheric delamination in the mature stages of continental collision, as well as lithospheric thinning announcing continental rifting in post-orogenic settings [3,4].

Andalusite is quite common in the pre-Alpine continental crust of the Alps, even if the age of the andalusite-bearing assemblages and the geological context in which they formed are various (Figure 1, Table 1). Andalusite-bearing rocks are associated with late-Variscan aplites, pegmatites, granitoids, and cordierite-bearing migmatites in the Helvetic

Argentera–Mercantour and Aiguilles Rouges massifs and often found in the contact zone of the Permian–Carboniferous intrusives [5–8]. Similarly, andalusite relics are found in the surroundings of late-Variscan granitoids in the Penninic Gran Paradiso massif [9] and in the pre-Permian metapelites of the Grand St. Bernard [10,11]. In the Penninic Briançon Basement, andalusite is instead related to a Permian thermal rise [12,13].

Different geological and chronological settings for andalusite development are envisaged in the Austroalpine and Southalpine domains, where andalusite-bearing assemblages testifying to Permian–Triassic lithospheric thinning are described together with older Permian–Carboniferous andalusite in the contact zone of late-Variscan intrusives [14–49]. In the Southalpine domain, andalusite mostly occurs in high-temperature basement rocks that include sillimanite, cordierite, and/or spinel that reflect Permian–Triassic Buchan/Abukuma-type metamorphism. In the upper Val Camonica, andalusite is instead found in chloritoid–staurolite–garnet-bearing metapelites, which suggest higher P/T conditions as characteristic of Barrovian/Dalradian metamorphism [1,2]. This case study thus represents an excellent opportunity to improve our understanding of the Variscan basement exhumation path, from the Variscan convergence to the Permian–Triassic lithospheric thinning. To this purpose, we present new multiscale structural data integrated with a detailed mineral–chemical and petrologic analysis, including thermodynamic modeling, aimed at identifying the geodynamic significance of the chloritoid–staurolite–andalusite transition in the upper Val Camonica basement.

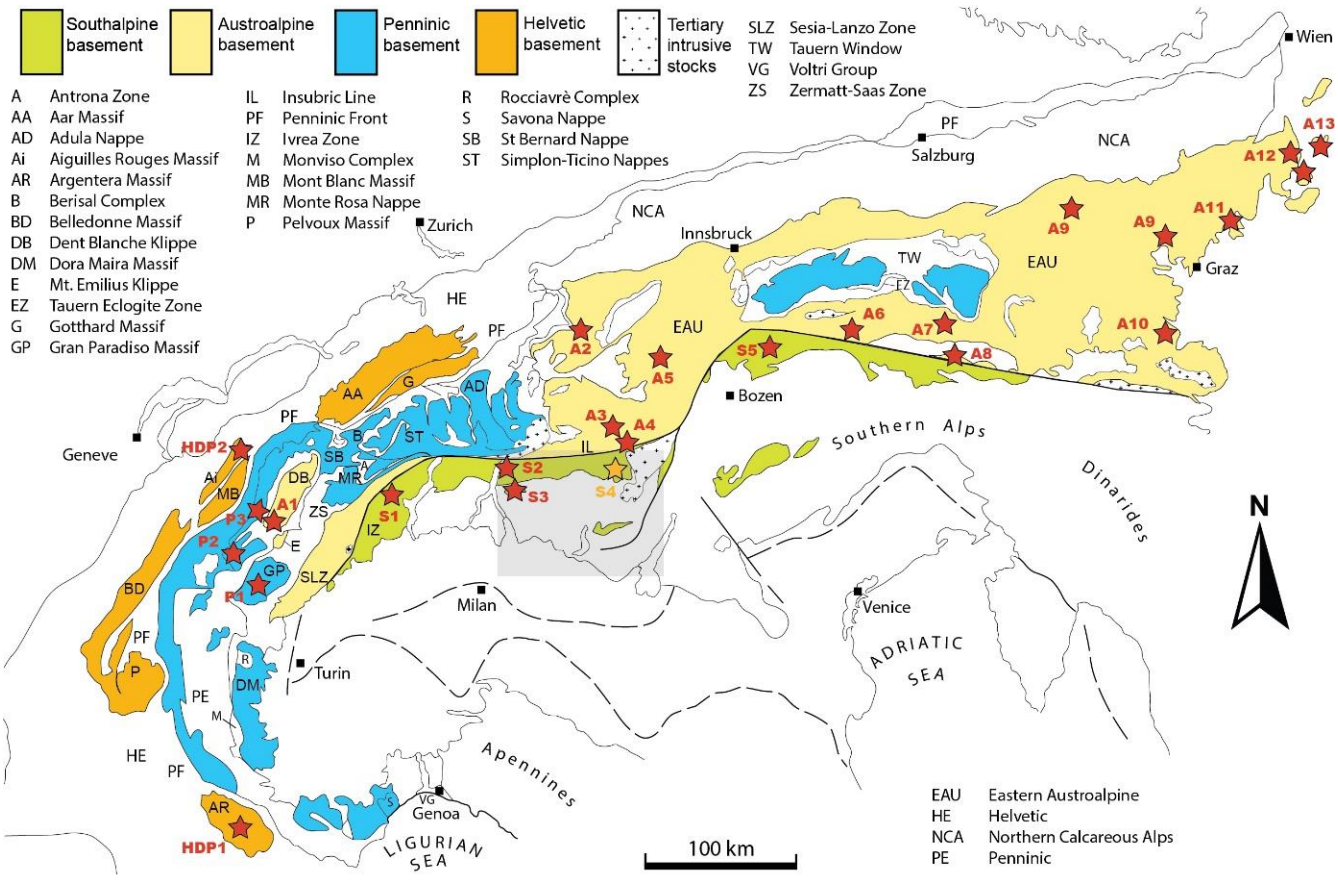

Figure 1. Tectonic map of the Alps redrawn following [50]. The red stars locate andalusite-bearing metapelites in the pre-Alpine basements; the orange star refers to the andalusite described in this work. Keys are coded in Table 1, where assemblages, inferred P-T conditions, and ages are listed with references. The grey shaded area locates the tectonic scheme of the central Southalpine domain proposed in Figure 2.

Table 1. Pre-Alpine andalusite-bearing assemblages in the continental crust of the Alps. Labels correspond to those of Figure 1. Mineral abbreviations follow [51]. When the radiometric method is not specified, the age is deduced from geological evidence or represents the average of results by different methods.

Tectonic System	Key	Location	Assemblage	T (°C)	P (GPa)	Age (Ma)	Method	Refs.
Helvetic—Dauphinois—Provençal	HDP 1	Argentera Massif Gesso Valley	And + Bt ± Sil ± Pl	-	-	292 ± 10, 299–296	Rb/Sr, Ar/Ar	[5,6,8]
Helvetic—Dauphinois—Provençal	HDP 2	Aiugilles Rouges Mieville	And + Ms + Tur ± Tpz ± Crd	-	-	Carboniferous–Permian	-	[7]
Penninic	P1	Gran Paradiso Pian Teleccio	Bt, Sil, Crn, Qz, Kfs, Pl, And?	-	-	Carboniferous–Permian	-	[9]
Penninic	P2	Briançon basement	And	450–550	0.1–0.3	Permian–Triassic (295–245)	Rb/Sr, K/Ar	[12,13]
Penninic	P3	Briançon Basement Mont Mort	Grt + Bt + Sil/And	550–600	0.5–0.8	332–328	U/Pb	[10,11]
Austroalpine	A1	Mont Mary Nappe	And + Ms	-	-	Permian	-	[23,28]
Austroalpine	A2	Silvretta Pischahorn	Qz + Ms + And	600	0.2	353–280, 353–295	Rb/Sr, K/Ar	[31]
Austroalpine	A3	Languard–Campo Sondalo	And + Crd	540	0.3–0.4	290–260	U/Pb	[39,46,47]
Austroalpine	A4	Languard–Campo	And + Ms	<500	<0.5	<250	U/Pb	[38,41,43,48]
Austroalpine	A5	Matsch Nappe	Grt + Sil/And + Bt ± Crd + Pl + Qz	570–640	0.30–0.55	Permian	Rb/Sr, U/Pb, Sm/Nd	[15,17,18]
Austroalpine	A6	Jenig Complex	And + Bt + Ms + Chl + Qz	450–530	0.24–0.42	254 ± 8	Sm/Nd	[19,20,37]
Austroalpine	A7	Kreuzeck Strieden Complex	And + Bt + Qz ± Pl ± Ms	500–570	<0.35	230–200	Ar/Ar	[24,37,40]
Austroalpine	A8	Deferegger Alps Uttenheim	And + Qz	-	-	>260, >290	Rb/Sr, Ar/Ar	[21,37]
Austroalpine	A9	Rappold Complex	(ex-) And	-	-	288 ± 4, 262 ± 2	Sm/Nd	[37,40]
Austroalpine	A10	Koralpe	(ex-) And	-	-	Permian–Triassic	-	[37,40]
Austroalpine	A11	Stralleg	And + Bt + Qz ± Pl ± Ms	550–600	0.32–0.48	Permian–Triassic	-	[37,40]
Austroalpine	A12	Sieggraben	(ex-) And	-	-	Permian–Triassic	-	[14,37,40]
Austroalpine	A13	Grobgneiss—Sopron	And + Bt ± Spl ± Ilm	575–620	0.18–0.25	330–320	K/Ar	[29,30,37,40]
Southalpine	S1	Strona–Ceneri Zone	Sill, And, Crd	-	-	Permian	-	[32,35]
Southalpine	S2	Dervio–Olgiasca Zone	And	< 600	<0.3	Triassic	-	[25,27,34,41,45]
Southalpine	S3	Val Biandino	And + Crd	500–600	<0.35	312 ± 48, 286 ± 20	Rb/Sr, K/Ar	[22,26,49]
Southalpine	S4	Val Camonica	And + Bt + Qz ± St	-	-	pre-Permian	-	[36], this work
Southalpine	S5	Isarco Valley	And + Bt + Crd	<670	0.25–0.35	282 ± 14	Rb/Sr	[16,33,42,44]

2. Geological Setting

The Variscan basement of the central Southalpine domain (i.e., the Orobic basement) comprises metapelites, gneisses, and quartzites, with minor metagranitoids, amphibolites, and marbles ([41,49,52–54] and refs. therein). The protoliths of these rocks mostly derive from Silurian–Ordovician sedimentary sequences and intrusives [55–57].

The dominant S2 foliation in the basement rocks is supported by greenschist facies minerals, which developed mainly during the late-collisional exhumation of the Variscan basement (>280 Ma, [49] and refs. therein), with few exceptions (e.g., [58,59] and refs. therein). S2 is truncated by siliciclastic Permian sequences, including conglomerates, arenites, and volcaniclastites, which are divided by unconformity in two cycles, dated lower- and mid-upper Permian, respectively [54,60–62]. The basement and sedimentary rocks were subsequently deformed and poorly metamorphosed during Alpine convergence (e.g., [63–65]), which was responsible for the development of D3 and D4 structures [56,66–69].

Mineral assemblages supporting precollisional and collisional Variscan structures (D1a, and D1b) are occasionally preserved in the Orobic basement, where five pre-Alpine Tectono–Metamorphic Units (TMUs) are distinguished [45,58] and shown in Figure 2:

1. the Val Vedello (VVB) and Monte Muggio Basements (MMB), in which kyanite–staurolite-bearing metapelites record the metamorphic peak of the Variscan collision under amphibolite facies conditions [25,53,70];
2. the Passo Cavalcafiche Basement (PCB) and Domaso–Cortafò Zone (DCZ), which record a prograde metamorphic evolution: syn-D1a chloritoid–garnet-bearing assemblages in metapelites testify to precollisional piling of cold lithospheric sheets under epidote–amphibolite facies conditions [71], whereas Syn-D1b staurolite–garnet-bearing assemblages formed during the subsequent Variscan collision [71];
3. the Aprica Basement (AB), which records two stages of the Variscan tectono–metamorphic evolution both under greenschist facies conditions, but marked by different P/T ratios [68]. A similar tectono–metamorphic evolution is also recorded in a small segment of Variscan basement immediately north of the Alpine Sellero line [55,58,72];
4. the Dervio–Olgiasca Zone (DOZ), which is the only TMU that records the high thermal state relatable to the "Tethyan rifting" at intermediate crustal depth [25,27]. Andalusite replacing sillimanite testifies to exhumation under high T/P ratio [25,52,73,74]. The Triassic age of this event is constrained by syn-D2 pegmatite ages [25,34,70,75]; and
5. the Tre Valli Bresciane (TVB) massif, where peak epidote–amphibolte facies conditions are recorded by chloritoid–garnet-bearing assemblages in metapelites [72,76].

In addition, P-T trajectories obtained from metamorphic pebbles from conglomerates of the lower Permian sedimentary cycle have been compared with the P-T evolutions inferred in different units of the Variscan basement [49,72,77]. In particular, metamorphic conditions retained by staurolite–garnet-bearing pebbles of basement rocks in the Aga and Vedello Conglomerates (AVC) (Figure 2) are similar to those characterizing the neighboring VVB and AB [77]. In the same way, metamorphic conditions retained by garnet–chloritoid-bearing pebbles in the Dosso dei Galli Conglomerate (DGC) (Figure 2) match those of the closest TVB [72].

In the siliciclastic Ponteranica Formation (POC, Figure 2), two types of pebbles are distinguished: the first type is similar to those found in the Aga and Vedello conglomerates, whereas, the second type contains andalusite-bearing assemblages interpreted either as developed during late-Variscan contact metamorphism, as induced by the emplacement of Val Biandino pluton, or during late-orogenic thermal relaxation [49].

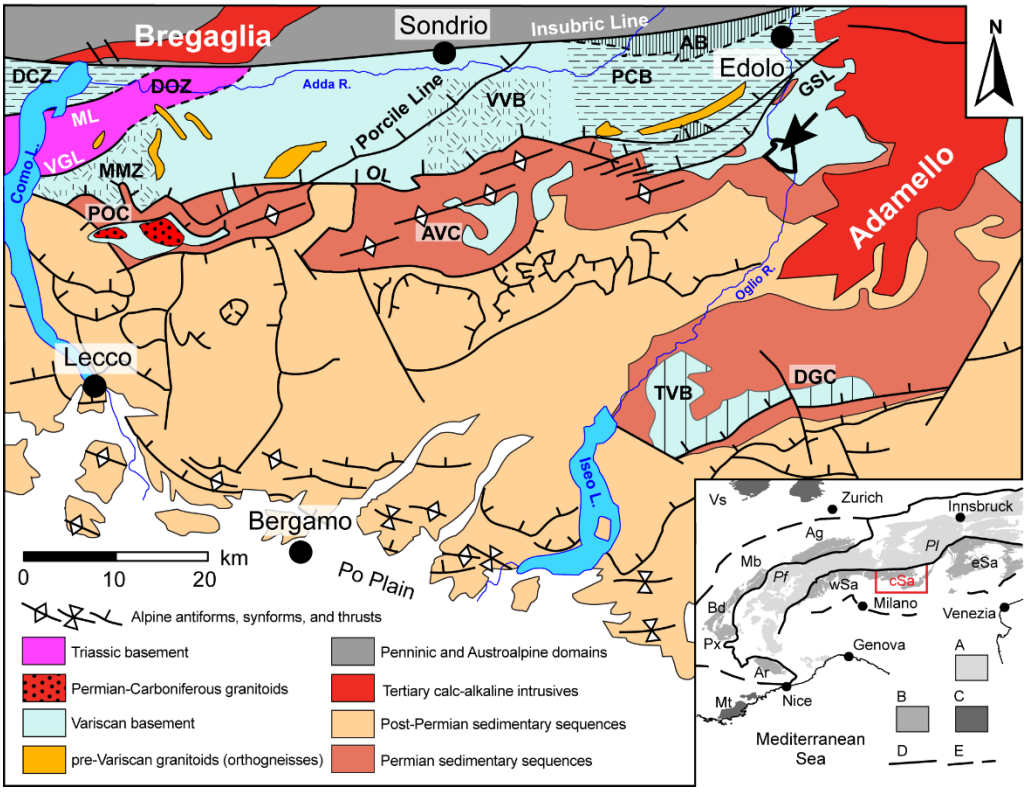

Figure 2. Geologic sketch of the central Southalpine domain modified from [49] and refs. therein. The present study area is shown as a black polygon indicated by a black arrow (cfr. Figure 3). Variscan Tectono–Metamorphic Units: AB = Aprica Basement; DCZ = Domaso—Cortafò Zone; DOZ = Dervio—Olgiasca Zone; MMZ = Monte Muggio Zone; PCB = Passo Cavalcafiche Basement; TVB = Tre Valli Bresciane massif; VVB = Val Vedello Basement. Permian conglomerates with pebbles deriving from the Variscan TMUs: POC = Ponteranica Formation; AVC = Aga and Vedello Conglomerates; DGC = Dosso dei Galli Conglomerate. Main tectonic lines: GSL = Gallinera e Sellero Lines; ML = Musso Line; OL = Orobic Line; VGL = Val Grande Line. Inset with the tectonic sketch of the Alps after [78]. A = Variscan basement rocks in the Alpine subduction complex; B = Variscan basement rocks in the Alpine external domains (Ag: Aar–Gotthard Massif, Ar: Argentera–Mercantour Massif, Bd: Belledonne Massif, Mb: Mont Blanc Massif, Px: Pelvoux Massif, wSa: western Southern Alps, cSa: central Southern Alps, eSa: eastern Southern Alps); C = Variscan basement rocks external to the Alpine fronts (Mt: Maures–Tanneron Massif, Vs: Vosges); D = lithospheric-scale structures delimiting the axial zone of the Alps (Pf: Penninic Front, Pl: Periadriatic Lineament); E: Alpine fronts.

The mid-upper Permian Verrucano Lombardo is part of the second sedimentary cycle capping most of the Orobic basement; it consists of poorly stratified fluvial conglomerates and sandstones ([62] and refs. therein) that grade into shallow sea deposits (Servino Formation) in early Triassic times [79]. This contribution focuses on a segment of the Orobic basement just below the Gallinera Line footwall (Figure 2), in upper Val Camonica. Here, the Verrucano Lombardo formation truncates late-collisional S2 in the exhumed Variscan basement.

3. Lithostratigraphy and Deformation History

Structural mapping was carried out on the right sloping bank of the Oglio river in upper Val Camonica, west of Cedegolo and Sellero villages (Figure 3). The aim was to constrain the intersection relationship between different types of pre-D2 structures in the Variscan basement. The Sellero–Cedegolo Basement, hereafter named SCB, mostly consists of chloritoid–staurolite-bearing metapelites, with minor lenses of garnet-bearing metagranitoids, paragneisses, and amphibolites, and is capped by the mid-upper Permian

Verrucano Lombardo. The relevance of this area in the Orobic basement is the outstanding occurrence of pre-Permian andalusite in the metapelites (Figure 3).

Four generations of superposed structures are distinguished in the SCB. In the metapelites, S2 foliation is supported by white mica, chlorite, ±albite (Figure 4). S2 dips from northwest to southeast, due to successive Alpine folding and thrusting (D3). Alpine D3 folds are characterized by southwest trending axes and steeply dipping axial planes (Figure 5).

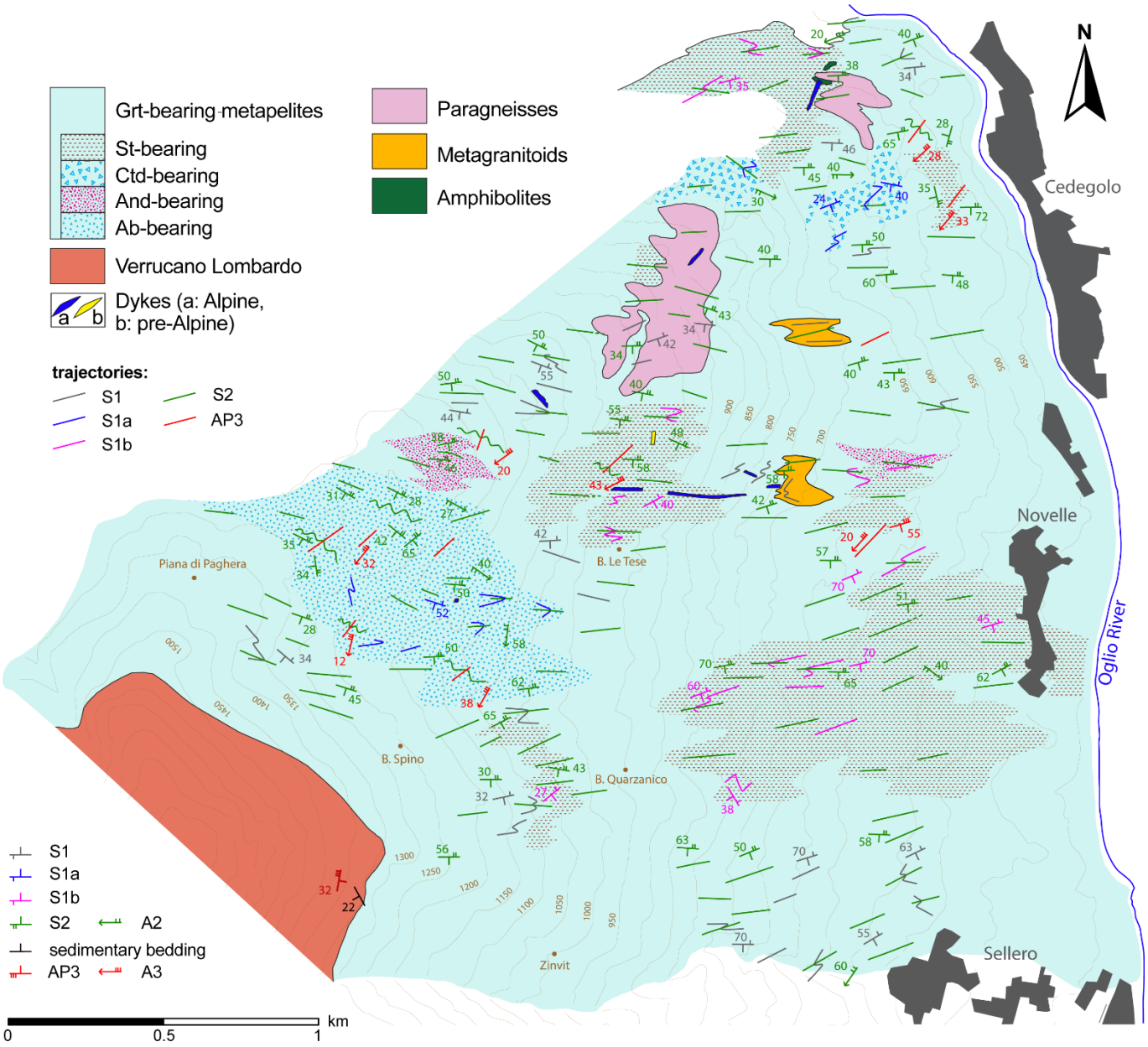

Figure 3. Interpretative structural map of the area west of Cedegolo and Sellero villages in the upper Val Camonica (location in Figure 2). Orientations of fabric elements synthesized in this foliation trajectory map are analytically shown in Figure 5. Urban areas are bounded by grey polygons.

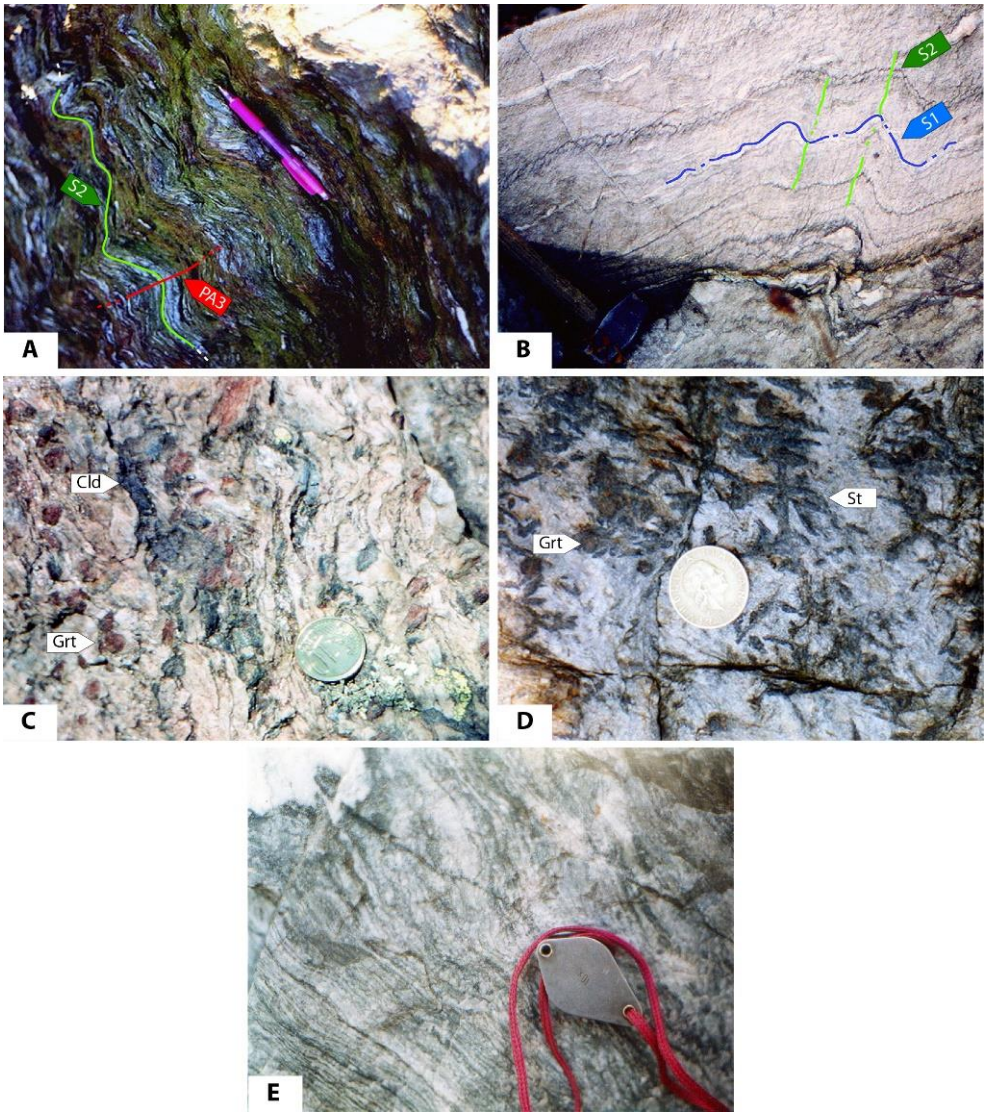

Figure 4. Mesoscale representative structures and mineral assemblages in the Sellero–Cedegolo basement. Metapelites: (**A**) Alpine D3 folding overprints Variscan S2 foliation marked by greenschist facies minerals. D3 axial plane dips to NW; (**B**) overprinting relationships between S1 and S2. S2 dips to S; (**C**) garnet (Grt) and chloritoid (Cld) grains supporting S1a foliation; (**D**) aggregates of staurolite (St) grains lying with garnet (Grt) on S1b foliation. Metagranitoids: (**E**) mylonitic S2 marked by chlorite and white mica. The red line is the lens lanyard, here used as scale.

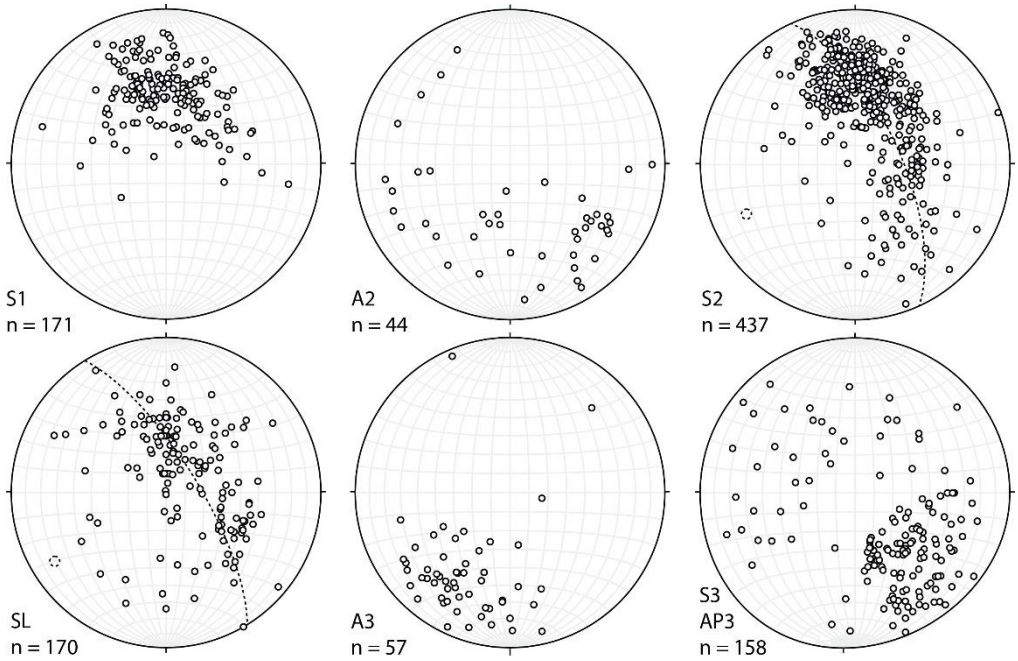

Figure 5. Schmidt stereographic projections (equal-area, lower hemisphere) of structural data, including Variscan (S1, S2) and Alpine (S3) poles to foliations, Variscan (A2) and Alpine (A3) fold axes and axial planes (AP3), and Permian sedimentary bedding (SL). Data are distinguished on relative chronology. Dotted lines and poles represent cylindrical best fits.

Pre-D2 foliations, S1a and S1b, are occasionally preserved in the area, even if mostly transposed into S2 (Figure 5). S1a is supported by white mica, garnet, biotite, and ± chloritoid, and S1b is supported by white mica, garnet, biotite, and ± staurolite (Figure 4). Overprinting relationships between S1a and S1b were not observed at the outcrop scale. On the basis of chloritoid or staurolite, S1 is demarcated as S1a or S1b, respectively. Where both intersection relationships and contrasting assemblages are absent, pre-D2 fabrics have been simply labeled S1.

In the metagranitoids, K-feldspar relics were wrapped by two superposed foliations: S1 was supported by biotite, white mica, plagioclase, and quartz and wraps rare garnet porphyroclasts. New white mica, chlorite, and rare plagioclase grains marked pervasive S2 (Figure 4E). Metric lenses of amphibolites were hosted within the staurolite-bearing metapelites in the northern part of the area (Figure 3). In the amphibolites, pervasive S2 was supported by amphibole, chlorite, quartz, epidote, and plagioclase; relict S1 was supported by amphibole, epidote, and biotite. Rare garnet porphyroclasts were found in the amphibolites.

The mid-upper Permian Verrucano Lombardo Formation unconformably covers the basement rocks and cuts S2 at the western boundary of the mapped area (Figure 3). D3 folds affect the basement rocks together with the Permian–Mesozoic sedimentary sequences. In both Variscan basement rocks and covers, D3 folds were characterized by a disjunctive axial plane foliation S3. S3 was marked by chlorite, white mica, and opaque minerals.

4. Microstructure and Mineral Chemistry

Deformation versus mineral growth relationships were determined for metapelites and metagranitoids that well preserved pre-D2 structures (Figure 6). The aim is to investigate the relationships between mineral growth and superposed fabrics and infer a robust P–T–d–t (Pressure–Temperature–deformation–time) path. The above described and regionally valid deformation history has been useful to individuate the site for investigating mineral compositional variations, taking into account: (a) the timing of mineral growth with respect to superposed fabric elements and (b) deformation mechanisms acting during the same deformation stage (e.g., [80–82]).

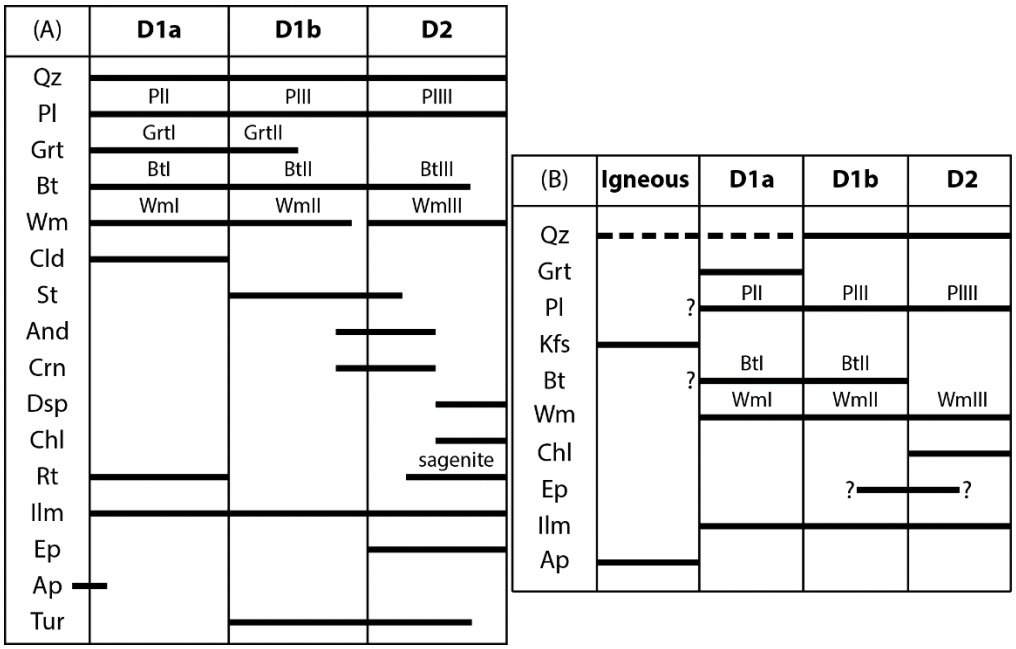

Figure 6. Deformations stages versus mineral growth in metapelites (**A**) and metagranitoids (**B**). Mineral abbreviations are from [51].

Mineral chemical analyses and backscattered electron (BSE) images were performed with the JEOL JXA-8200 electron microprobe in wavelength dispersion mode (EMPA) at the laboratory of the Department of Earth Sciences of the University of Milan, Italy, under the following conditions: 15 kV accelerating voltage, 5 nA beam current, and a count time of 60 s on peak and 30 s on the background, with a 1 μm diameter beam. Natural minerals were used as standards and the rough data corrected for matrix effects using a conventional φρZ routine in the JEOL software. Compositional parameters of the analyzed minerals in metapelites and metagranitoids are reported in Table 2. The mineral chemical dataset is attached in Table S1 (Supplementary Materials).

Table 2. Synthesis of mineral chemical analyses. Stoichiometric formulae are calculated as follows: garnet at 8 cations and 12 oxygen atoms, epidote at 8 cations and 12.5 oxygen atoms, biotite and white mica at 22 oxygen atoms, chloritoid at 12 oxygen atoms, staurolite at 46 oxygen atoms, chlorite at 7 oxygen atoms, and plagioclase at 4 oxygen atoms. Average values are in brackets.

Rock Type	Stage	Mineral	Alm	Prp	Grs	Si	Al	Pg	Fe + Mg	Ti	X_{Mg}	An	Ab
Metapelites	D1a	Grt I	0.75–0.90 (0.81)	0.01–0.10 (0.05)	0.05–0.20 (0.14)								
		Wm I				6.21–6.38	5.39–5.72	0.03–0.20	0.13–0.43				
		Bt I								0.17–0.25	0.19–0.29		
		Pl I										4–5	94–96
		Cld									0.04–0.11		
	D1b	Grt II	0.86–0.94 (0.89)	0.02–0.10 (0.06)	0.02–0.07 (0.04)								
		Wm II				6.10–6.20	5.67–5.90	0.08–0.28	0.07–0.23				
		Bt II								0.10–0.23	0.30–0.40		
		Pl II										21–22	77–78
		St									0.06–0.15		
	D2	Wm III				5.91–5.94	5.95–6.02	0.09–0.10	0.05–0.06				
		Pl III				-	-					1–3	97–98
		Chl (And)				2.44–2.53	2.98–3.18				0.36–0.38		
		Chl (Cld)				2.53–2.69	2.90–3.11				0.17–0.29		
		Chl (Grt)				2.44–3.01	2.44–3.05				0.09–0.37		
		Chl (St)				2.49–2.64	2.93–3.05				0.34–0.46		
Meta-granitoids	D1a	Grt	0.58–0.62 (0.60)	0.03	0.35–0.39 (0.37)								
		Wm I				6.11–6.27	5.22–5.38	0.08–0.11	0.34–0.48				
		Bt I								0.28–0.38	0.30–0.34		
		Pl I										13–42	56–86
	D1b	Wm II				6.20–6.47	4.88–5.42	0.08–0.12	0.33–0.69				
		Bt II								0.21	0.33		
		Pl II										2–6	92–97

4.1. Metapelites

S1a and S1b are well preserved in the selected metapelites. S1a is supported by shape-preferred orientation (SPO) of white mica (WmI, Si > 6.20 apfu), chloritoid (X_{Mg} = 0.04–0.11), biotite (BtI, X_{Mg} = 0.19–0.29), quartz, rutile, and ilmenite. These minerals, with rare grains of plagioclase (PlI, $An_{4–5}$), mark the internal foliation of millimeter- to centimeter-sized garnet porphyroblasts (GrtI, $Alm_{81}Grs_{14}Prp_5$). Inclusion patterns in GrtI are usually straight, slightly curved at garnet rims, and continuous with the external S1a foliation. Similarly, millimeter-sized chloritoid grains included S1a as internal foliation (Figure 7A).

S1a is crenulated by D1b and, where S1b is well developed, decussate and plastically deformed WmI and BtI crystals are preserved in microlithons and/or as rotated grains in the cleavage domains. GrtI cores contain internal S1a, discordant with external S1b (Figure 7B), and show thin inclusion-free rims (GrtII, $Alm_{89}Grs_6Prp_4$). S1b is marked by white mica (WmII, 6.10 $\leq$ Si $\leq$ 6.20 apfu with Pg < 0.20), staurolite (X_{Mg} = 0.06–0.15), biotite (BtII, X_{Mg} = 0.30–0.40), and ilmenite; quartz and plagioclase (PlII, $An_{21–22}$) occupy the microlithons. Skeletal GrtII grains are in trails along S1b together with staurolite. Overprinting of staurolite-bearing S1b on chloritoid-bearing S1a is exceptionally preserved (Figure 7A); in addition, staurolite includes S1b foliation deflected into strain caps around GrtI porphyroclasts (Figure 7B), or it fills the necks of microboudinaged chloritoid grains (Figure 7C).

S1b is crenulated by D2 or microfaulted along localized shear bands. S2 is outlined by chlorite, white mica (WmIII, Si = 5.91–5.94 apfu, Pg = 0.09–0.10), ilmenite, tourmaline, and rare biotite (BtIII). Plastically deformed grains of biotite and white mica were re-oriented along S2. Centimeter-sized plagioclase crystals (PlIII, $An_{1–3}$) retain S2 as internal foliation. Plagioclase porphyroclasts are statically replaced by epidote and sericite, whereas chlorite overgrew garnet, chloritoid, and staurolite.

Andalusite crystals of millimeter to centimeter size include S1b as internal foliation, either straight, curved, or gently folded by D2 (Figure 7D,E), but continuous with external S1b. Andalusite was microboudinaged during D2, with WmIII, BtIII, and chlorite filling the boudin necks, and wrapped by coronae of very fine-grained WmIII. These features suggest that andalusite growth took place during the final stages of S1b development and ceased during early-D2. Staurolite inclusions are recurrent in andalusite grains and display sharp grain boundaries (Figure 7F). Andalusite locally forms aggregates with small corundum grains. In most cases, corundum is rimmed by diaspore (Figure 7G,H).

The following mineral compositional evolutions are here summarized and highlighted in Figure 8 and Table 2: (1) replacement of Ca by Fe^{2+} from GrtI to GrtII; (2) decrease in Si and Mg + Fe content from WmI to WmII to WmIII; (3) increase in X_{Mg} from BtI to BtII; (4) increase in An component from PlI to PlII and decreasing from PlII to PlIII. Chlorite composition seems to be controlled by the microstructural site: chlorite replacing andalusite and staurolite has X_{Mg} = 0.34–0.36, chlorite replacing chloritoid has X_{Mg} = 0.17–0.29, chlorite rimming garnet shows X_{Mg} = 0.09–0.37 and the lowest Al content (Figure 8).

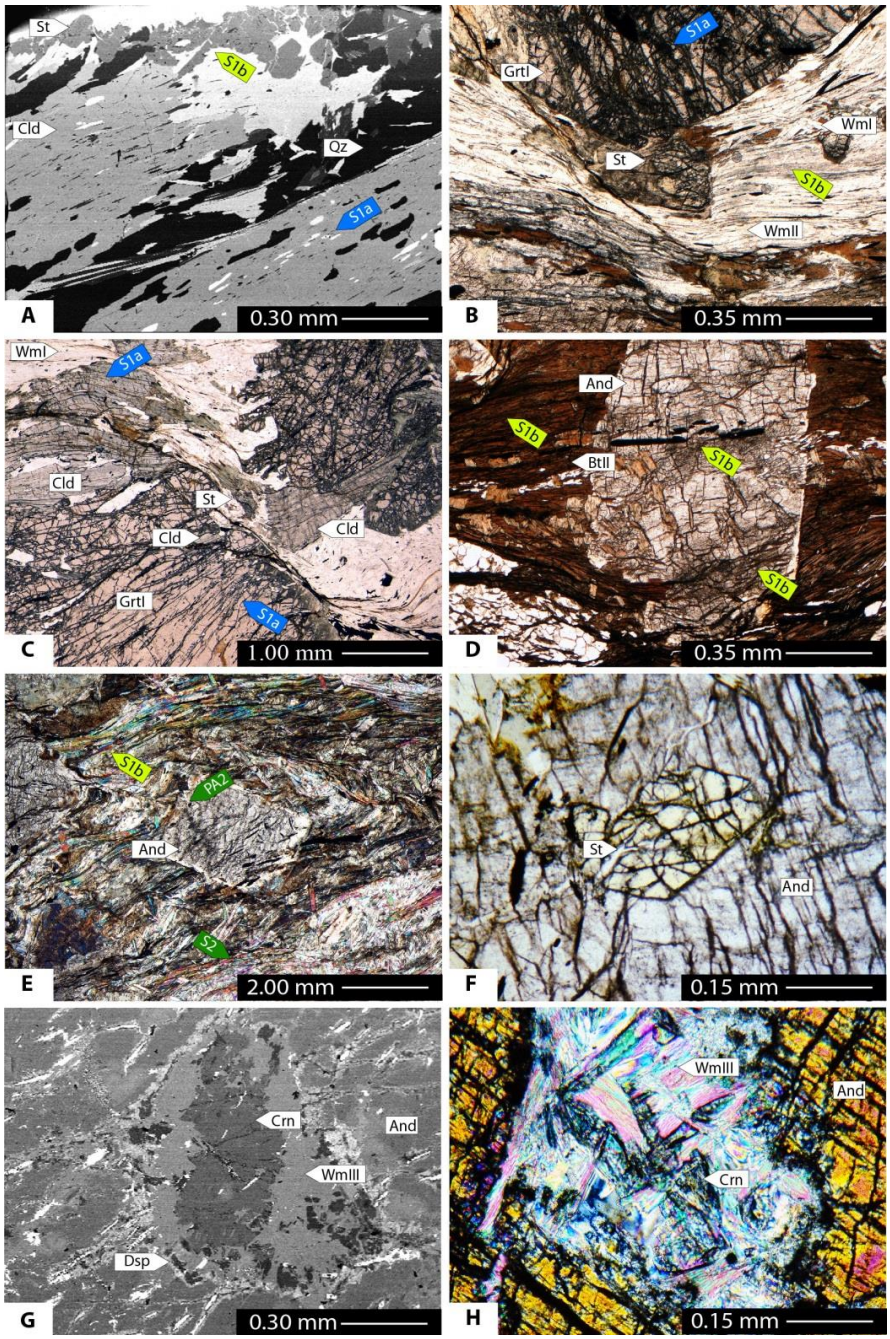

Figure 7. Variscan metapelites. (**A**) S1a supported by shape-preferred orientation of millimeter-sized chloritoid porphyroblasts (BSE image). Internal foliation in chloritoid is continuous with external S1a. S1b is supported by submillimeter sized staurolite grains and cuts S1a. (**B**) Porphyroclast of GrtI wrapped by S1b. S1b is marked by WmII and BtII. GrtI retains a straight internal foliation discontinuous with the external one. Staurolite in the strain caps around GrtI encloses deflected S1b (PPL image). (**C**) S1a supported by chloritoid. Chloritoid is included in GrtI, and the internal foliation in both GrtI and chloritoid is deflected but continuous with the external foliation S1a. Chloritoid grains are boudinaged and staurolite grew in the boudin-neck (PPL image). (**D**) Andalusite with internal foliation continuous with external S1b: the internal foliation is straight at the grain core and curved at the rim. S1b is marked by BtII. Decussate grains of biotite are preserved in cleavage domains and as inclusions in andalusite (PPL image). (**E**) Post-kinematic andalusite porphyroblast overprints D2 folds (PPL image). (**F**) Andalusite porphyroblast includes staurolite with equilibrium grain boundaries (PPL image). (**G**,**H**) Andalusite porphyroblasts include corundum grains and are replaced by diaspore and WmIII (BSE and XPL images).

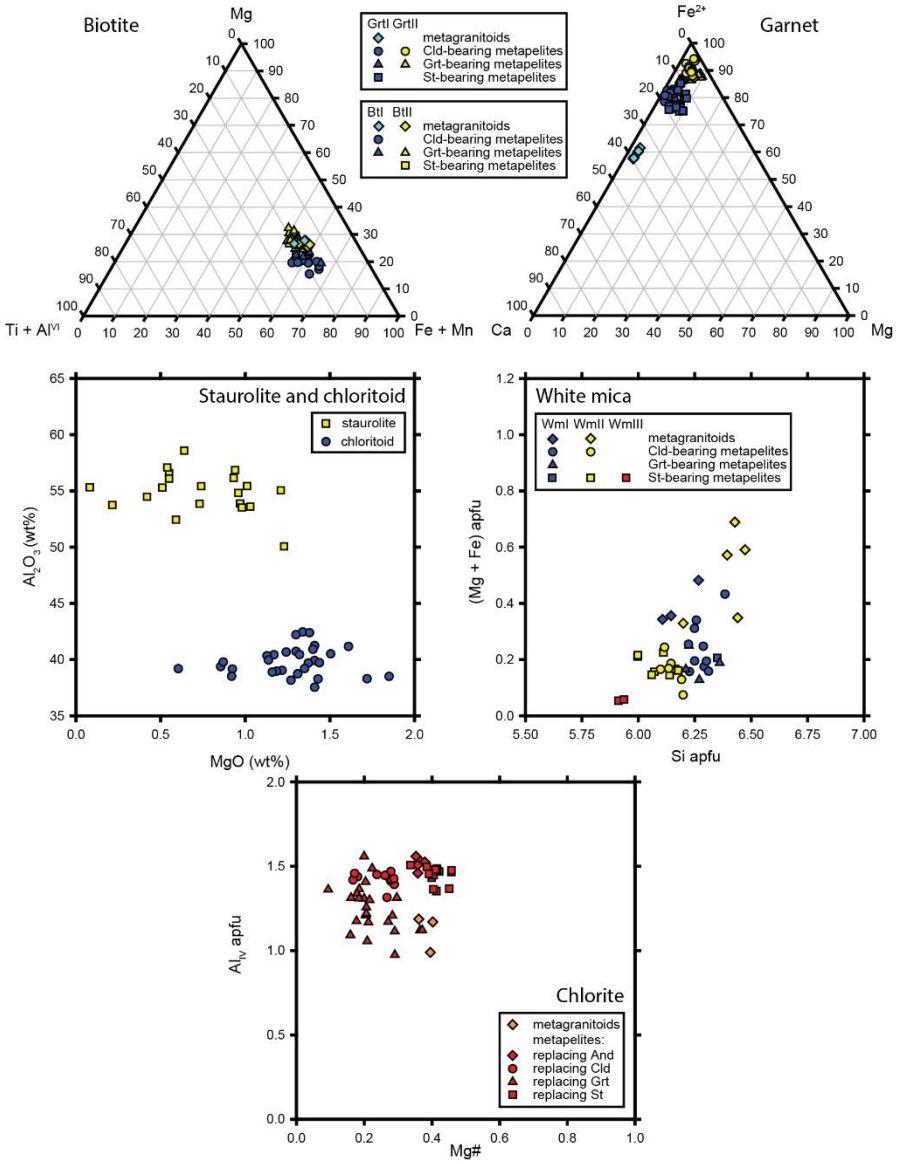

Figure 8. Compositional variations of the main rock-forming minerals in metapelites and metagranitoids as a function of rock-type (triangle: garnet-bearing metapelites, circle: chloritoid-bearing metapelites, square: staurolite-bearing metapelites) and microstructural site (D1a—blue, D1b—yellow, D2—red).

4.2. Metagranitoids

S2 is the dominant foliation in metagranitoids. S1a and S1b are locally preserved in low strained domains and wrap relics of igneous K-feldspar. S1b is supported by biotite (BtII, X_{Mg} = 0.33, Ti < 0.21 apfu), quartz, plagioclase (PlII, $An_{2–6}$), minor white mica (WmII, Si = 6.20–6.47 apfu, Pg < 0.12), and ilmenite. S1a is the internal foliation in skeletal garnet grains ($Alm_{51}Grs_{31}Prp_3Sps_{16}$) and is supported by elongated inclusions of quartz. In the garnet porphyrclasts, S1a is discontinuous with respect to the external foliation S1b. Decussate grains of biotite (BtI, X_{Mg} = 0.30–0.34, Ti = 0.28–0.38 apfu) and white mica (WmI, Si = 6.11–6.27 apfu, Pg < 0.11) were found in the microlithons, with an early generation of plagioclase (PlI, $An_{13–42}$) that is extensively replaced by white mica and epidote ($Fe^{3+}/(Al^{VI} + Fe^{3+})$ = 0.16–0.17). BtI, WmI, PlI, garnet, and quartz are considered stable during S1a development. Finally, S2 is supported by white mica, ilmenite, and chlorite (X_{Mg} = 0.36–0.40), which pervasively replace biotite and garnet.

5. Metamorphic Evolution vs. Deformation History

This section constrains the P-T conditions under which D1a, D1b, and D2 structures developed in the Variscan basement. The Permian sedimentary sequences overlying the SCB define a Permian age limit for the exhumation of the Variscan basement in upper Val Camonica.

Metamorphic conditions for the subsequent deformation stages recorded in the metapelites were estimated by means of thermobarometers and pseudosections. Temperatures were constrained using different Fe–Mg cationic exchange between mineral pairs in textural equilibrium. Chloritoid–biotite and chloritoid–garnet thermometry [83,84] was applied on mineral grains supporting S1a foliation and gave a temperature interval of 490–580 °C. Staurolite–garnet thermometry [80] on minerals marking S1b provided a temperature interval of 580–610 °C. The result was fully consistent with the upper stability of chloritoid in the $FeO–Al_2O_3–SiO_2–H_2O$ (FASH) system, which reacted to form staurolite and/or almandine by increasing the temperature above 550 °C ([85] and refs. therein). Garnet–biotite thermometry [86–89] coherently indicated that S1a developed at T = 480–540 °C and S1b at T = 510–630 °C. Pressure conditions were estimated by garnet–plagioclase–biotite–muscovite–quartz [90] and garnet–plagioclase–muscovite–quartz barometers [91]: S1a developed at P = 0.8–1.0 GPa and S1b at P = 0.4–0.6 GPa.

Pseudosections were calculated by the Theriak/Domino program [92] to better constrain the P-T intervals accountable for D1a, D1b, and early D2 events in metapelites and metagranitoids. We adopted a converted version of the self-consistent thermodynamic database ds55 [93] in the $CaO–Na_2O–K_2O–FeO–MgO–Al_2O_3–SiO_2–H_2O$ (CNKFMASH) system, including the following mineral activity-composition (a-x) relations: garnet [94], biotite [94], chlorite [95], white mica [96], chloritoid [95], and staurolite [95]. The selected bulk compositions were acquired from metapelite and metagranitoid samples from the lithostratigraphic unit in the Orobic basement that included the rocks analyzed in this work [93]. Mn was excluded, because it is negligible in the metapelites and only fractionated in garnet in the metagranitoids; P content is almost entirely contained in apatite and thus removed from the system together with stoichiometric Ca. Water was considered in excess except where indicated.

In the metapelites, the syn-D1a assemblage plagioclase + garnet + biotite + white mica + chloritoid + quartz was stable at T = 530–560 °C and P = 0.6–0.8 GPa (Figure 9A). The resulting stability field was delimited at low temperature and high pressure by chlorite-in and chloritoid-out curves, at high temperature by chloritoid-out and staurolite-in (T = 560 °C) curves, and at low-pressure by garnet-out curves. Within the D1a field, the garnet composition changed from $Alm_{79}Grs_{16}Prp_5$ to $Alm_{87}Grs_8Prp_5$ under increasing of the T/P ratio. The Si content in white mica is 6.20 apfu and consistent with $P \simeq 0.8$ GPa. The computed compositions matched those of GrtI ($Alm_{81}Grs_{14}Prp_5$) and WmI ($Si \geq 6.20$ apfu) in the metapelites for T = 530–550 °C and $P \simeq 0.8$ GPa.

The syn-D1b assemblage garnet + biotite + white mica + staurolite + quartz was stable at T = 560–650 °C and P = 0.5–0.7 GPa. The predicted stability field was delimited at high pressure by staurolite-out, at high temperature by univariant sillimanite-in/staurolite-out, and at low pressure by garnet-out. In this field, garnet is characterized by almandine content at around 0.90 and grossular at around 0.05, as in GrtII ($Alm_{89}Grs_6Prp_4$). This portion of the P-T space likely represents the main stage of S1b development, which was followed by further decompression and exhumation out of the garnet stability field, as suggested by the Si content in WmII ($6.10 \leq Si \leq 6.20$ apfu).

Andalusite was stable together with staurolite at T = 520–580 °C and P = 0.2–0.4 GPa (Figure 9B). These metamorphic conditions characterized the transition between D1b and D2 deformation stages. A further exhumation of metapelites towards shallower levels is testified to by the replacement of corundum by diaspore at $T \leq 400$ °C and $P \leq 0.2$ GPa [95].

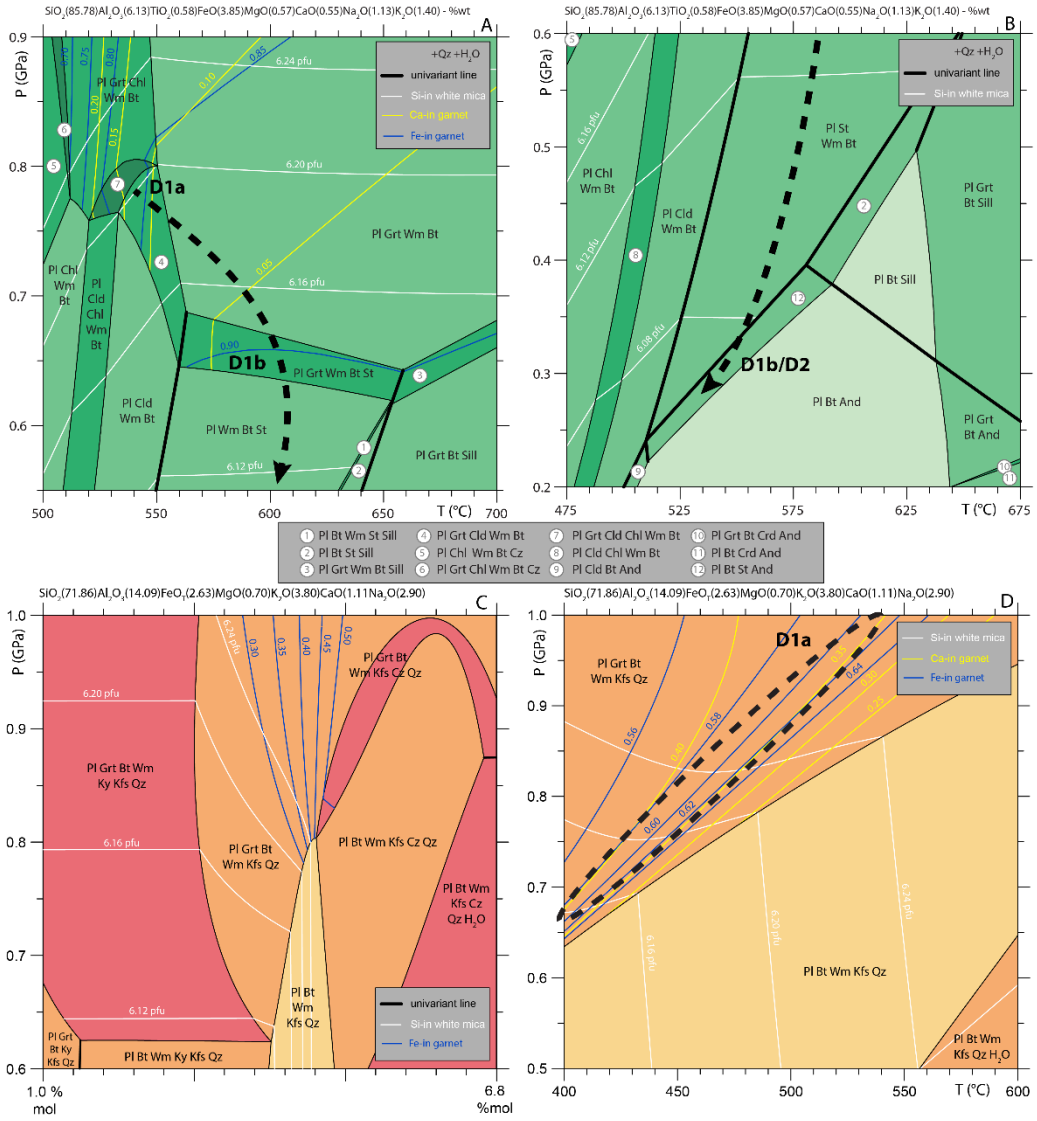

Figure 9. P-T and P-X pseudosections calculated in the CNKFMASH system for metapelites (**A**,**B**) and metagranitoids (**C**,**D**) in the SCB. Bulk compositions are from [97]. Fields are colored as function of variance. Si-in white mica, Ca-in garnet, and Fe-in garnet isopleths are added. P-T accountable for D1a to D2 deformation stages are highlighted by dotted ellipses and lines.

In the metagranitoids, the stability and composition of garnet was mostly controlled by the amount of water in the system (Figure 9C). Increasing water content, garnet was stable towards higher pressure at the same temperature. The analyzed garnet ($Alm_{60}Grs_{37}Prp_3$) was predicted in the Pl + Grt + Bt + Wm + Kfs + Qz field if considered in slightly undersaturated conditions (~3% mol of H_2O). The P-T conditions accountable for garnet development vary from 450 °C and 0.65 GPa to 530 °C and 1.00 GPa (Figure 9D). In this wide P-T interval, biotite X_{Mg} (0.30–0.38) matched with the analysis on Bt I (0.30–0.34) and the Si content in white mica (6.14–6.34 apfu) was comparable to that of Wm I (6.11–6.27 apfu). This modeling suggests that garnet stability in the metagranitoids is only possible at P-T conditions (T = 450–530 °C, P = 0.7–1.0 GPa), slightly cooler but comparable with those determined for D1a in the metapelites (T = 520–550 °C, P ≃ 0.8 GPa), and not during D1b, in agreement with the microstructural relationships.

6. Discussion and Conclusions

Multiscale structural analysis integrated with petrology in the SCB rocks allowed the reconstruction of the Variscan P–T–d–t evolution, predating the deposition of the Permian–Triassic sedimentary sequences (Figures 3 and 10, [54]). The Variscan structural evolution was testified to by the superposition of three groups of structures developed under different metamorphic conditions: D1a structures formed at the boundary between epidote amphibolite- and amphibolite-facies conditions (at T = 450–570 °C and P = 0.7–1.0 GPa), D1b under amphibolite-facies conditions, at higher temperature and slightly lower pressure (T = 550–650 °C and P = 0.4–0.7 GPa), whereas D2 structures are marked by mineral assemblages testifying to the transition towards greenschist-facies conditions ($T \leq 400$ °C and $P \leq 0.3$ GPa). Overprinting relationships between chloritoid–garnet-bearing S1a and staurolite–garnet-bearing S1b confirmed that the development of the various mineral assemblages was controlled by different thermal states during successive deformation stages.

The textural relationship between staurolite and andalusite in some of the SCB rocks suggests local equilibrium between the two minerals. Andalusite–staurolite assemblages developed at T = 520–580 °C and P = 0.2–0.4 GPa, during the transition from late D1b to early D2 stages. This is in contrast with the textural relationships in metamorphic clasts of the Lower Permian Ponteranica Formation that shows andalusite replacing staurolite [49].

The thermal state obtained by the syn-D1a P-T conditions (Figure 10) was characterized by a T/depth ratio of 15–18 °C·km^{-1} and plots between those of warm subduction zones, plate interior, and continental collision zones [98] and is compatible with tectonic piling of cold lithospheric sheets during the Variscan convergence, as already suggested in other portions of the Orobic basement and interpreted as an effect of the Variscan continental subduction and collision (e.g., PCB, DCZ, TVB [71,72]).

D1b structures developed under P-T_{max} conditions indicated a T/depth ratio of 25–30 °C·km^{-1} and suggested a thermal state compatible with that of plate interior [98]. This thermal state is compatible with those of the Variscan continental collision, in agreement with other tectono–metamorphic units in the Southalpine domain (e.g., VVB, MMB, PCB, and DCZ [25,49,53,59,68,70,71,77]).

Andalusite–staurolite-bearing assemblages developed under T/depth ratio comprised between 40 and 70 °C·km^{-1} in between late-D1b and early-D2 indicate that a high thermal state was already effective at the end of the exhumation trajectory of the SCB rocks. The stratigraphic contact with the Verrucano Lombardo Formation in the area, and with lower Permian sequences few kilometers north of SCB, makes the greenschist-facies D2 structures older than Permian ([49,54] and refs. therein). Any relationship with the Permian–Triassic high thermal state that characterized the DOZ [25,52,73,74] is precluded, since the SCB was already exhumed at that time. The identified high thermal state is thus interpreted as related to a Variscan late-orogenic thinning, associated with lithospheric delamination. This interpretation is supported by the predictions of 2D numerical models (Figure 10) performed for simulating a subduction and collision process, whose convergence rate is set by paleogeographic constraints on the Variscan belt [99–101].

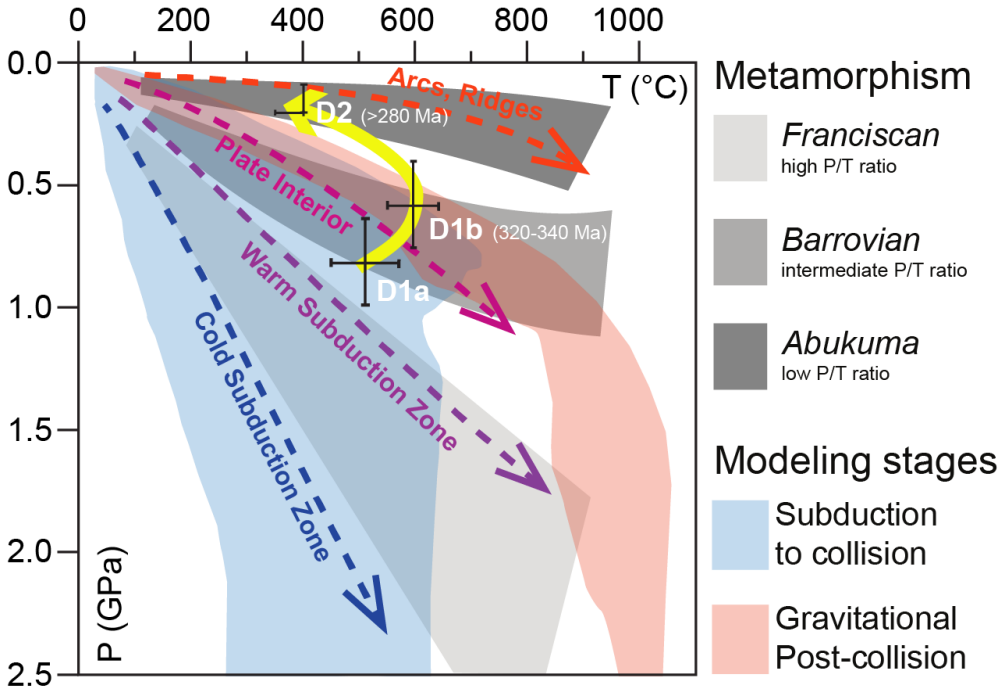

Figure 10. Comparison between the P-T path inferred for the SCB rocks (yellow line with arrow), metamorphic field gradients, and P-T predictions obtained during different stages of a 2D numerical model of Variscan convergence (subduction/post-collisional stages ([99] and refs. therein). Cross signs refer to the P-T conditions attained by the SCB rocks during D1a to D2 deformation stages. Dashed geotherms "Arcs, Ridges", "Plate Interior", "Warm Subduction Zones", and "Cold Subduction Zones" follow [98]. D1a, D1b, and D2 refer to the metamorphic conditions related to the successive groups of structures in SCB. Ages referred to D1b and D2 are inferred from radiometric and stratigraphic data ([49,62,102] and refs. therein).

The inferred evolution makes unique this portion of the Southalpine basement with respect to the other units, where the thermal record of the late-collisional evolution is instead registered at deeper crustal levels, as testified by sillimanite and/or cordierite with andalusite [42,44,49,103,104]. This contribution indicates that the high thermal regime affecting Southalpine basement rocks during pre-Alpine times may also result from late-Variscan orogenic collapse and not only by Permian–Triassic lithospheric thinning. The superimposition of such an elevated thermal state in the pre-Alpine basement suggests that the thermal softening of the continental lithosphere at the end of the Variscan convergence may have led to the localization of Permian–Triassic weakened zones in the Alpine area.

Supplementary Materials: The following are available online at https://www.mdpi.com/article/10.3390/min11101124/s1, Table S1: Mineral chemical analysis.

Author Contributions: Conceptualization, M.F. and M.I.S.; fieldwork and microstructure, M.F., N.P., M.I.S. and D.Z.; mineral chemistry, M.F., N.P., V.D. and M.I.S.; petrologic modeling, M.F. and J.-M.L.; visualization, M.F., M.I.S., V.D.; writing–original draft, M.F., M.I.S., V.D., J.-M.L. and D.Z. All authors have read and agreed to the published version of the manuscript.

Funding: This research was funded by GECT (CTE_INT16DZANO_M) and Universitá di Milano—Linea B (PSR2020_MRODA).

Data Availability Statement: Not Applicable.

Acknowledgments: We acknowledge Curzio Malinverno for thin section preparation and Andrea Risplendente for support with the electron microprobe. We thank G. Gosso and G.B. Siletto for fruitful discussion and suggestions.

Conflicts of Interest: The authors declare no conflict of interest.

References

1. Miyashiro, A. Evolution of metamorphic belts. *J. Petrol.* **1961**, *2*, 277–311. [CrossRef]
2. Regorda, A.; Spalla, M.I.; Roda, M.; Lardeaux, J.-M.; Marotta, A.M. Metamorphic facies and deformation fabrics diagnostic of subduction: Insights from 2D numerical models. *Geochem. Geophys.* **2021**. [CrossRef]
3. Thompson, A.B. The pressure-temperature (P, T) plane viewed by geophysicists and petrologists. *Terra Cognita* **1981**, *1*, 11–20.
4. Schuster, R.; Stüwe, K. Permian metamorphic event in the Alps. *Geology* **2008**, *36*, 603–606. [CrossRef]
5. Ferrara, G.; Malaroda, R. Radiometric age of granitic rocks from the Argentera Massif (Maritime Alps). *Boll. Soc. Geol. It.* **1969**, *88*, 311–320.
6. Compagnoni, R.; Lombardo, B.; Prato, R. Andalousite et sillimanite aux contacts du Granite Central de l'Argentera (Alpes Maritimes). *Rend. Soc. Ital. Mineral. Petrol.* **1974**, *39*, 31–54.
7. Brändlein, P.; Nollau, G.; Sharp, Z.; von Raumer, J.F. Petrography and geochemistry of the Vallorcine granite (Aiguilles Rouges massif, Western Alps). *Schweiz. Mineral. Petrogr. Mitt.* **1994**, *74*, 227–243.
8. Corsini, M.; Ruffet, G.; Caby, R. Alpine and late-hercynian geochronological constrains in the Argentera Massif (Western Alps). *Eclogae Geol. Helv.* **2004**, *97*, 3–15. [CrossRef]
9. Compagnoni, R.; Prato, R. Paramorfosi di cianite su sillimanite in scisti pregranitici del Massiccio del Gran Paradiso. *Boll. Soc. Geol. It.* **1969**, *88*, 537–549.
10. Bussy, F.; Sartori, M.; Thélin, P. U-Pb zircon dating in the middle Penninic basement of the Western Alps (Valais, Switzerland). *Schweiz. Mineral. Petrogr. Mitt.* **1996**, *76*, 81–84.
11. Giorgis, D.; Thélin, P.; Stampfli, G.; Bussy, F. The Mont-Mort metapelites: Variscan metamorphism and geodynamic context (Brianconnais basement, western Alps, Switzerland). *Schweiz. Mineral. Petrogr. Mitt.* **1999**, *79*, 381–398.
12. Bocquet, J.; Delaloye, M.; Hunziker, J.C.; Krummenacher, D. K–Ar and Rb-Sr dating of blue amphiboles, micas and associated minerals from the western Alps. *Contrib. Mineral. Petrol.* **1974**, *47*, 7–26. [CrossRef]
13. Desmons, J. The Briancon basement (Pennine Western Alps): Mineral composition and polymetamorphic evolution. *Schweiz. Mineral. Petrogr. Mitt.* **1992**, *72*, 37–55.
14. Beck-Mannagetta, P. Über den geologischen Aufbau der Koralpe. *Verh. Geol. B.-A.* **1970**, *3*, 491–496.
15. Gregnanin, A. Metamorphism and magmatism in the western Italian Tyrol. *Rend. Soc. Ital. Mineral. Petrol.* **1980**, *36*, 49–64.
16. Del Moro, A.; Visonà, D. The epiplutonic Hercynian Complex of Brixen (Bressanone, Eastern Alps, Italy). Petrologic and radiometric data. *Neu. Jb. Mineral. Abh.* **1982**, *145*, 66–85.
17. Haas, R. Zur Metamorphose des Suedlichen Oetztalkristallins unter Besonderer Beruecksichtigung der Matscher Einheit (Vintschgau/Suedtirol). Ph.D. Thesis, Innsbruck University, Innsbruck, Austria, 1985.
18. Habler, G.; Thöni, M.; Grasemann, B. Cretaceous metamorphism in the Austroalpine Matsch Unit (Eastern Alps): The interrelation between deformation and chemical equilibration processes. *Mineral. Petrol.* **2009**, *97*, 149–171. [CrossRef]
19. Philippitsch, R.; Malecki, G.; Heinz, H. Andalusit-Granat-Staurolith-Glimmerschiefer im Gailtalkristallin (Kärnten). *Jb. Geol. B.-A.* **1986**, *129*, 93–98.
20. Schuster, R.; Tropper, P.; Krenn, E.; Finger, F.; Frank, W.; Philippitsch, R. Prograde Permo-Triassic metamorphic HT/LP assemblages from the Austroalpine Jenig Complex (Carinthia Austria). *Austrian J. Earth Sci.* **2015**, *108*, 73–90. [CrossRef]
21. Stoeckhert, B. Das Uttenheimer Pegmatitfeld (Ostalpines Altkristallin, Südtirol). Genese und alpine Überprägung. *Erlanger Geol. Abh.* **1987**, *114*, 83–106.
22. De Capitani, L.; Delitala, M.C.; Liborio, G.; Mottana, A.; Nicoletti, M.; Petrucciani, C. K–Ar dating of the Val Biandino plutonic complex (Orobic Alps, Italy). *Mem. Sci. Geol. Univ. Padova* **1988**, *40*, 285–294.
23. Canepa, M.; Castelletto, M.; Cesare, B.; Martin, S.; Zaggia, L. The Austroalpine Mont Mary nappe (Italian Western Alps). *Mem. Sci. Geol. Univ. Padova* **1990**, *42*, 1–17.
24. Hoke, L. The Altkristallin of the Kreuzeck Mountains, SE Tauern Window, Eastern Alps—Basement Crust in a Convergent Plate Boundary Zone. *Jb. Geol. B.-A.* **1990**, *133*, 5–87.
25. Diella, V.; Spalla, M.I.; Tunesi, A. Contrasting thermomechanical evolutions in the Southalpine metamorphic basement of the Orobic Alps (Central Alps, Italy). *J. Metamorph. Geol.* **1992**, *10*, 203–219. [CrossRef]
26. Thöni, M.; Mottana, A.; Delitala, M.C.; De Capitani, L.; Liborio, G. The Val Biandino composite pluton: A Late Hercynian intrusion into the South Alpine metamorphic basement of the Alps (Italy). *Neues Jahrb. Mineral. Monatshefte* **1992**, *12*, 545–554.
27. Bertotti, G.; Siletto, G.B.; Spalla, M.I. Deformation and metamorphism associated with crustal rifting: The Permian to Liassic evolution of the Lake Lugano-Lake Como area (Southern Alps). *Tectonophysics* **1993**, *226*, 271–284. [CrossRef]
28. Dal Piaz, G.V. Evolution of Austroalpine and Upper Penninic basement in the Northwestern Alps from Variscan convergence to post-Variscan extension. In *Pre-Mesozoic Geology in the Alps*; von Raumer, J.F., Neubauer, F., Eds.; Springer: Heidelberg, Germany, 1993; pp. 325–342.
29. Balogh, K.; Dunkl, I. K/Ar dating of metamorphic rocks from the Sopron Mts., Lower Austro-Alpine Unit (Hungary). *Mitt. Österr. Mineral. Gesell.* **1994**, *139*, 26–27.
30. Török, K. Pre-Alpine development of the andalusite–sillimanite–biotite–schist from the Sopron Mountains (Eastern Alps, Western Hungary). *Acta Geol. Hung.* **1999**, *42*, 127–160.
31. Brugger, J. Les veines à andalousite du Pischahorn (Grisons, Suisse). *Schweiz. Mineral. Petrogr. Mitt.* **1994**, *74*, 191–202.

32. Boriani, A.; Burlini, L. *Carta Geologica della Valle Cannobina Scala 1:25000*; Dipartimento di Scienze della Terra, Università di Milano: Milano, Italy, 1995.
33. Visonà, D. Polybaric evolution of calc-alkaline magmas: The dioritic belt of the Bressanone-Chiusa igneous complex (NE Italy). *Mem. Sci. Geol. Univ. Padova* **1995**, *47*, 11–124.
34. Sanders, C.A.; Bertotti, G.; Tommasini, S.; Davies, G.R.; Wijbrans, J.R. Triassic pegmatites in the Mesozoic middle crust of the Southern Alps (Italy): Fluid inclusions, radiometric dating and tectonic implications. *Eclogae Geol. Helv.* **1996**, *89*, 505–526.
35. Colombo, A.; Tunesi, A. Pre-Alpine metamorphism of the Southern Alps west of the Giudicarie Line. *Schweiz. Mineral. Petrogr. Mitt.* **1999**, *79*, 63–77.
36. Diella, V.; Pigazzini, N.; Gosso, G.; Siletto, G.B.; Spalla, M.I. New occurrence of Cld-And-bearing metapelites in the Southalpine basement of the upper Val Camonica. *Geol. Paläont. Mitt. Innsbruck* **2001**, *25*, 68–69.
37. Schuster, R.; Scharbert, S.; Abart, R.; Frank, W. Permo-Triassic extension and related HT/LP metamorphism in the Austroalpine-Southalpine realm. *Mitt. Ges. Geol. Bergbaustud. Oesterr.* **2001**, *45*, 111–141.
38. Spalla, M.I.; Zucali, M.; Salvi, F.; Gosso, G.; Gazzola, D. Tectono-metamorphic map of the Languard-Campo, Serie del Tonale Nappes between Upper Val Camonica and Valtellina (Central Italian Alps, Austroalpine domain). *Mem. Sci. Geol. Univ. Padova* **2003**, *55*, 105–118.
39. Gosso, G.; Engi, M.; Koller, F.; Lardeaux, J.M.; Oberhaensli, R.; Spalla, M.I. *Thermo-Mechanical Evolution of the Alpine Belt, from the Engadine Window to the Matterhorn. 32nd IGC Field Trip Guidebook*; APAT: Rome, Italy, 2004; Volume B29, pp. 1–52.
40. Schuster, R.; Koller, F.; Hoeck, V.; Hoinkes, G.; Bousquet, R. Metamorphic evolution of the Eastern Alps. *Mitt. Österr. Mineral. Gesell.* **2004**, *149*, 175–199.
41. Spalla, M.I.; Zucali, M.; di Paola, S.; Gosso, G. A critical assessment of the tectono-thermal memory of rocks and definition of tectono-metamorphic units: Evidence from fabric and degree of metamorphic transformations. *Geol. Soc. London Spec. Publ.* **2005**, *243*, 227–247. [CrossRef]
42. Benciolini, L.; Poli, M.E.; Visonà, D.; Zanferrari, A. Looking inside Late Variscan tectonics: Structural and metamorphic heterogeneity of the Eastern Southalpine Basement (NE Italy). *Geodin Acta* **2006**, *19*, 17–32. [CrossRef]
43. Salvi, F.; Spalla, M.I.; Zucali, M.; Gosso, G. Three-dimensional evaluation of fabric evolution and metamorphic reaction progress in polycyclic and polymetamorphic terrains: A case from the Central Italian Alps. *Geol. Soc. Lond. Spec. Publ.* **2010**, *332*, 173–187. [CrossRef]
44. Wyhlidal, S.; Thöny, W.F.; Tropper, P.; Kaindl, R.; Hauzenberger, C.; Mair, V. Petrology of contact metamorphic metapelites from the southern rim of the Permian Brixen Granodiorite (South Tyrol, Italy). *Mineral. Petrol.* **2012**, *106*, 173–191. [CrossRef]
45. Spalla, M.I.; Zanoni, D.; Marotta, A.M.; Rebay, G.; Roda, M.; Zucali, M.; Gosso, G. The transition from Variscan collision to continental break-up in the Alps: Insights from the comparison between natural data and numerical model predictions. *Geol. Soc. Lond. Spec. Publ.* **2014**, *405*, 363–400. [CrossRef]
46. Petri, B.; Mohn, G.; Štípská, P.; Schulmann, K.; Manatschal, G. The Sondalo Gabbro contact aureole (Campo Unit, Eastern Alps): Implications for mid-crustal mafic magma emplacement. *Contrib. Mineral. Petrol.* **2016**, *171*, 52. [CrossRef]
47. Petri, B.; Mohn, G.; Skrzypek, E.; Mateeva, T.; Galster, F.; Manatschal, G. U-Pb geochronology of the Sondalo Gabbroic Complex (Central Alps) and its position within the Permian post-Variscan extension. *Int. J. Earth Sci.* **2017**, *106*, 2873–2893. [CrossRef]
48. Roda, M.; Zucali, M.; Li, Z.X.; Spalla, M.I.; Yao, W. Pre-alpine contrasting tectono-metamorphic evolutions within the Southern Steep Belt, Central Alps. *Lithos* **2018**, *310*, 31–49. [CrossRef]
49. Zanoni, D.; Spalla, M.I. The Variscan evolution in basement cobbles of the Permian Ponteranica Formation by microstructural and petrologic analysis. *Ital. J. Geosci.* **2018**, *137*, 254–271. [CrossRef]
50. Spalla, M.I.; Marotta, A.M. P-T evolutions vs. numerical modelling: A key to unravel the Paleozoic to early-Mesozoic tectonic evolution of the Alpine area. *Period. Mineral.* **2007**, *76*, 267–308.
51. Whitney, D.L.; Evans, B.W. Abbreviations for names of rock-forming minerals. *Am. Mineral.* **2010**, *95*, 185–187. [CrossRef]
52. Mottana, A.; Nicoletti, M.; Petrucciani, C.; Liborio, G.; De Capitani, L.; Bocchio, R. Pre-alpine and alpine evolution of the Southalpine basement of the Orobic Alps. *Geol. Rundsch.* **1985**, *74*, 353–366. [CrossRef]
53. Siletto, G.B.; Spalla, M.I.; Tunesi, A.; Lardeaux, J.M.; Colombo, A. Pre-Alpine structural and metamorphic histories in the Orobic southern Alps, Italy. In *Pre-Mesozoic Geology in the Alps*; von Raumer, J.F., Neubauer, F., Eds.; Springer: Heidelberg, Germany, 1993; pp. 585–598.
54. Gosso, G.; Spalla, M.I.; Bini, A.; Siletto, G.B.; Berra, F.; Forcella, F. *Note Illustrative della Carta Geologica d'Italia alla Scala 1:50.000, Foglio 057 Malonno*; ISPRA and Regione: Lombardia, Italy, 2012.
55. Gansser, A.; Pantič, N. Prealpine events along the Eastern Insubric Line (Tonale Line, northern Italy). *Eclogae Geol. Helv.* **1988**, *81*, 567–577.
56. Milano, P.F.; Pennacchioni, G.; Spalla, M.I. Alpine and pre-Alpine tectonics in the Central Orobic Alps (Southern Alps). *Eclogae Geol. Helv.* **1988**, *81*, 273–293.
57. Colombo, A.; Siletto, G.B.; Tunesi, A. Pre-Variscan magmatism in the central Southern Alps: The Monte Fioraro magmatic complex. *Schweiz. Mineral. Petrogr. Mitt.* **1994**, *74*, 127–135.
58. Spalla, M.I.; Gosso, G. Pre-Alpine tectonometamorphic units in the central Southern Alps: Structural and metamorphic memory. *Mem. Sci. Geol. Univ. Padova* **1999**, *51*, 221–229.

59. Di Paola, S.; Spalla, M.I.; Gosso, G. New structural mapping and metamorphic evolution of the Domaso Cortafo Zone (Southern Alps-Lake Como). *Mem. Sci. Geol. Univ. Padova* **2001**, *53*, 1–14.
60. Cassinis, G.; Dal Piaz, G.V.; Eusebio, A.; Gosso, G.; Martinotti, G.; Massari, F.; Milano, P.F.; Pennacchioni, G.; Perello, M.; Pessina, C.M.; et al. Report on a structural and sedimentological analysis in the Uranium Province of the Orobic Alps. *Uranium* **1986**, *2*, 241–260.
61. Cadel, G.; Cosi, M.; Pennacchioni, G.; Spalla, M.I. A new map of the Permo-Carboniferous cover and Variscan metamorphic basement in the Central Orobic Alps, Southern Alps—Italy. *Mem. Sci. Geol. Univ. Padova* **1996**, *48*, 1–53.
62. Berra, F.; Felletti, F.; Tessarollo, A. Stratigraphic architecture of a transtensional continental basin in low-altitude semiarid conditions: The Permian succession of the central Orobic basin (Southern Alps, Italy). *J. Sediment. Res.* **2016**, *86*, 408–429. [CrossRef]
63. Wennekers, J.H.L. The structure of the Bergamo Alps compared with that of the Highlands of Scotland. *Leidse Geol. Meded.* **1932**, *4*, 83–93.
64. Crespi, R.; Liborio, G.; Mottana, A. On a widespread occurrence of stilpnomelane to the South of the Insubric line, Central Alps, Italy. *Neues Jahrb. Mineral. Monatshefte* **1982**, *6*, 265–271.
65. Laubscher, H.P. Large scale thin-skin thrusting in the Southern Alps. *Geol. Soc. Am. Bull.* **1985**, *96*, 710–718. [CrossRef]
66. Albini, S.; Battaglia, D.; Bellini, G.; Bigoni, C.; Carminati, E.; Ceriani, S.; Forcella, F.; Gosso, G.; Guizzetti, A.; Oliva, G.; et al. Alpine deformations and pre-Alpine remnants in the north-eastern Orobic Alps, Southalpine Belt. *Quad. Geodin. Alp. Quat.* **1994**, *2*, 25–39.
67. Carminati, E.; Siletto, G.B.; Battaglia, D. Thrust kinematics and internal deformation in basement involved foreland fold and thrust belts: The Eastern Orobic Alps case (Central Southern Alps, Northern Italy). *Tectonics* **1997**, *16*, 259–271. [CrossRef]
68. Rebay, G.; Maroni, M.; Siletto, G.B.; Spalla, M.I. Superposed syn-metamorphic structures of the Alpine and pre-Alpine convergent cycles in the Southalpine basement of the Orobic Alps (Northern Italy). *J. Maps* **2015**, *11*, 168–180. [CrossRef]
69. Zanchetta, S.; Malusà, M.G.; Zanchi, A. Precollisional development and Cenozoic evolution of the Southalpine retro-belt (European Alps). *Lithosphere* **2015**, *7*, 662–681.
70. Gosso, G.; Siletto, G.B.; Spalla, M.I. International ophiolite symposium field excursion guide-continental rifting to ocean floor metamorphism (21st–23rd September 1995): First day: HT/LP metamorphism and structures in the South-Alpine basement near Lake Como, Orobic Alps; intracontinental imprints of the Permo-Triassic rifting. *Ofioliti* **1997**, *22*, 133–145.
71. Spalla, M.I.; Carminati, E.; Ceriani, S.; Oliva, A.; Battaglia, D. Influence of deformation partitioning and metamorphic re-equilibration on P–T path reconstruction in the pre-Alpine basement of central Southern Alps (Northern Italy). *J. Metamorph. Geol.* **1999**, *17*, 319–336. [CrossRef]
72. Spalla, M.I.; Zanoni, D.; Gosso, G.; Zucali, M. Deciphering the geologic memory of a Permian conglomerate of the Southern Alps by pebble P–T estimates. *Int. J. Earth Sci.* **2009**, *98*, 203–226. [CrossRef]
73. Di Paola, S.; Spalla, M.I. Contrasting tectonic records in pre-Alpine metabasites of the Southern Alps (Lake Como, Italy). *J. Geodyn.* **2000**, *30*, 167–189. [CrossRef]
74. Spalla, M.I.; Siletto, G.B.; di Paola, S.; Gosso, G. The role of structural and metamorphic memory in the distinction of tectono-metamorphic units: The basement of the Como lake in the Southern Alps. *J. Geodyn* **2000**, *30*, 191–204. [CrossRef]
75. Real, C.; Froitzheim, N.; Carosi, R.; Ferrando, S. Evidence of large-scale Mesozoic detachments preserved in the basement of the Southern Alps (northern Lago di Como area). *Ital. J. Geosci.* **2018**, *137*, 283–293. [CrossRef]
76. Giobbi Origoni, E.; Gregnanin, A. The crystalline basement of the "Massiccio delle Tre Valli Bresciane": New petrographic and chemical data. *Mem. Soc. Geol. Ital.* **1983**, *26*, 133–144.
77. Zanoni, D.; Spalla, M.I.; Gosso, G. Vestiges of lost tectonic units in conglomerate pebbles? A test in Permian sequences of the Southalpine Orobic Alps. *Geol. Mag.* **2010**, *147*, 98–122. [CrossRef]
78. Filippi, M.; Zanoni, D.; Gosso, G.; Lardeaux, J.M.; Verati, C.; Spalla, M.I. Structure of lamprophyres: A discriminant marker for Variscan and Alpine tectonics in the Argentera-Mercantour Massif, Maritime Alps. *BSGF-Earth Sci. Bull.* **2019**, *190*, 12. [CrossRef]
79. Sciunnach, D.; Garzanti, E.; Confalonieri, M.P. Stratigraphy and petrography of Upper Permian to Anisian terrigenous wedges (Verrucano Lombardo, Servino and Bellano formations; western southern Alps). *Riv. Ital. Paleontol. Stratigr.* **1996**, *102*, 27–48.
80. Spalla, M.I.; Zucali, M. Deformation vs. metamorphic reequilibration heterogeneities in polymetamorphic rocks: A key to infer quality P-T-d-t path. *Period. Mineral.* **2004**, *73*, 249–257.
81. Passchier, C.W.; Trouw, R.A. *Microtectonics*; Springer: Berlin/Heidelberg, Germany, 2005; p. 366.
82. Gosso, G.; Rebay, G.; Roda, M.; Spalla, M.I.; Tarallo, M.; Zanoni, D.; Zucali, M. Taking advantage of petrostructural heterogeneities in subduction-collisional orogens and effect on the scale of analysis. *Period. Mineral.* **2015**, *84*, 779–825.
83. Perchuck, L.L. PT-fluid regimes of metamorphism and related magmatism with specific reference to the granulite-facies Sharyzhalgay complex of Lake Baikal. *Geol. Soc. London Spec. Publ.* **1989**, *43*, 275–291. [CrossRef]
84. Perchuck, L.L. Derivation of thermodynamically consistent set of geothermometers and geobarometers for metamorphic and magmatic rocks. In *Progress in Metamorphic and Magmatic Petrology. A Memorial Volume in Honor of D.S. Korzhinskiy*; University Press Cambridge: Cambridge, UK, 1991; pp. 93–112.
85. Spear, F.S. *Metamorphic Phase Equilibria and Pressure-Temperature-Time Paths*; Mineralogical Society of America Monograph: Chantilly, VA, USA, 1995; p. 799.

86. Holdaway, M.J.; Lee, S.M. Fe-Mg cordierite stability in high-grade pelitic rocks based on experimental, theoretical, and natural observations. *Contrib. Mineral. Petrol.* **1977**, *63*, 175–198. [CrossRef]
87. Ferry, J.T.; Spear, F.S. Experimental calibration of the partitioning of Fe and Mg between biotite and garnet. *Contrib. Mineral. Petrol.* **1978**, *66*, 113–117. [CrossRef]
88. Perchuck, L.L.; Lavrent'eva, I.V. Experimental investigation of exchange equilibria in the system cordierite-garnet-biotite. In *Kinetics and Equilibrium in Mineral Reactions. Advances in Physical Geochemistry*; Saxena, S.K., Ed.; Springer: Berlin/Hiedelberg, Germany, 1983; Volume 3, pp. 199–239.
89. Holdaway, M.J. Application of new experimental and garnet Margules data to the garnet-biotite geothermometer. *Am. Mineral.* **2000**, *85*, 881–892. [CrossRef]
90. Ghent, E.D.; Stout, M.Z. Geobarometry and geothermometry of plagioclase-biotite-garnet-muscovite assemblages. *Contrib. Mineral. Petrol.* **1981**, *76*, 92–97. [CrossRef]
91. Hodges, K.V.; Crowley, P.T. Error estimation and empirical geothermobarometry for pelitic systems. *Am. Mineral.* **1985**, *70*, 702–709.
92. De Capitani, C.; Petrakakis, K. The computation of equilibrium assemblage diagrams with Theriak/Domino software. *Am. Mineral.* **2010**, *95*, 1006–1016. [CrossRef]
93. Holland, T.J.B.; Powell, R. Activity-composition relations for phases in petrological calculations: An asymmetric multicomponent formulation. *Contrib. Mineral. Petrol.* **2003**, *145*, 492–501. [CrossRef]
94. White, R.W.; Powell, R.; Holland, T.J.B. Progress relating to calculation of partial melting equilibria for metapelites. *J. Metamorph. Geol.* **2007**, *25*, 511–527. [CrossRef]
95. Holland, T.J.B.; Powell, R. An internally consistent thermodynamic dataset for phases of petrological interest. *J. Metamorph. Geol.* **1998**, *16*, 309–343. [CrossRef]
96. Coggon, R.; Holland, T.J.B. Mixing properties of phengitic micas and revised garnet-phengite thermobarometers. *J. Metamorph. Geol.* **2002**, *20*, 683–696. [CrossRef]
97. Caironi, V.; Colombo, A.; Tunesi, A. Geochemical approach to characterization and source identification of the protoliths of metasedimentary rocks: An example from the Southern Alps. *Period. Mineral.* **2004**, *73*, 109–118.
98. Cloos, M. Lithospheric buoyancy and collisional orogenesis: Subduction of oceanic plateaus, continental margins, island arcs, spreading ridges, and seamounts. *Geol. Soc. Am. Bull.* **1993**, *105*, 715–737. [CrossRef]
99. Regorda, A.; Roda, M.; Marotta, A.M.; Spalla, M.I. 2-D numerical study of hydrated wedge dynamics from subduction to post-collisional phases. *Geophys. J. Int.* **2017**, *211*, 952–978. [CrossRef]
100. Von Raumer, J.F.; Stampfli, G.M.; Bussy, F. Gondwana-derived microcontinents—The constituents of the Variscan and Alpine collisional orogens. *Tectnophysics* **2003**, *365*, 7–22. [CrossRef]
101. Marotta, A.M.; Spalla, M.I. Permian-Triassic high thermal regime in the Alps: Result of late Variscan collapse or continental rifting? Validation by numerical modeling. *Tectonics* **2007**, *26*, 1–27. [CrossRef]
102. Regorda, A.; Lardeaux, J.M.; Roda, M.; Marotta, A.M.; Spalla, M.I. How many subductions in the Variscan orogeny? Insights from numerical models. *Geosci. Front.* **2020**, *11*, 1025–1052. [CrossRef]
103. Boriani, A.; Caironi, V.; Oddone, M.; Vannucci, R. Some petrological and geochemical constraints on the genesis of the Baveno-Mottarone and Montorfano plutonic bodies. *Rend. Soc. Ital. Mineral. Petrol.* **1988**, *43*, 385–393.
104. Boriani, A.; Giobbi, E. Does the basement of western southern Alps display a tilted section through the continental crust? A review and discussion. *Period Miner.* **2004**, *73*, 5–22.